International Journal of Modern Physics B
Vol. 30, No. 3 (2016) 1550263 (11 pages)

DOI: 10.1142/S021797921550263X

Analytical calculation of electron group velocity surfaces in uniform strained graphene

Wilfrido A. Gómez-Arias* and Gerardo G. Naumis†

Departamento de Física-Química, Instituto de Física,
Universidad Nacional Autónoma de México (UNAM),
Apartado Postal 20-364, 01000 México, Distrito Federal, México
**wilantgomari@fisica.unam.mx*
†*naumis@fisica.unam.mx*

Received 11 September 2015
Revised 22 October 2015
Accepted 30 October 2015
Published 24 December 2015

Electron group velocity for graphene under uniform strain is obtained analytically by using the tight-binding (TB) approximation. Such closed analytical expressions are useful in order to calculate the electronic, thermal and optical properties of strained graphene. These results allow to understand the behavior of electrons when graphene is subjected to strong strain and nonlinear corrections, for which the usual Dirac approach is no longer valid. Some particular cases of uniaxial and shear strain were analyzed. The evolution of the electron group velocity indicates a break-up of the trigonal warping symmetry, which is replaced by a warping consistent with the symmetry of the strained reciprocal lattice. To do this, analytical expressions for the shape of the first Brillouin zone (BZ) of the honeycomb strained reciprocal lattice are provided. Finally, the Fermi velocity becomes strongly anisotropic, i.e., for a strong pure shear strain (20% of the lattice parameter), the two inequivalent Dirac cones merge and the Fermi velocity is zero in one of the principal axis of deformation. We found that nonlinear terms are essential to describe the effects of deformation for electrons near or at the Fermi energy.

Keywords: Graphene; strain; group velocity.

PACS numbers: 73.22.Pr, 77.80.bn, 81.05.ue

1. Introduction

Graphene was the first two-dimensional (2D) crystal discovered.[1] It has been broadly studied due to the observed peculiar physical properties.[2–5] The electronic properties are mainly determined by electrons at the Fermi energy.[4] For graphene,

*Corresponding author.

such electrons have momentum near or at the high symmetry points of Brillouin zone (BZ). This behavior can be modeled by a Dirac Hamiltonian,[6] where electrons behave as massless Dirac fermions with a Fermi velocity $v_F \simeq 1 \times 10^6$ m/s, which plays the role of the speed of light. In this model, the Fermi velocity is a constant parameter. However, this is no longer true when graphene has corrugations (curved space) or is stretched, since these deformations give rise to a space-dependent Fermi velocity,[7] suggesting changes in the electronic conductivity. Furthermore, in the case of stretching or periodic strain, a band-gap opening is observed.[7–12] Such results open the possibility for doing "strain engineering" in order to tailor the electronic properties and thus control the electron transport.[13–17]

Several theoretical approaches have been proposed to study deformations in graphene.[6,18–24] The most common one is a combination of the tight-binding (TB) Hamiltonian and linear elasticity to derive a Dirac effective equation.[6] Under such approach, pseudomagnetic fields appear, although lattice deformations were not included in the original derivation.[25] In the case of strain, recent works have included these considerations starting from different treatments.[16,20,25,26] Still, there are some problems with such approach[27] because a common confusion is the assumption that the Dirac cone tips $\mathbf{K}_D$ in the new deformed lattice coincides with the strained high symmetry points $\mathbf{K}$ and $\mathbf{K}'$.

For example, in the usual pseudomagnetic field approach,[28] the case of a uniform strain is not well reproduced.[27] This case turns out to be simple benchmark tool to test theories of strain on graphene since it can be solved by other means in a straight forward manner.[27] To do so, consider a simple isotropic stretching of the lattice, which can be written as $\boldsymbol{\epsilon} = \epsilon \mathbf{I}$, where $\boldsymbol{\epsilon}$ is the strain tensor, given by a constant ϵ multiplied by the unitary matrix $\mathbf{I}$. This stretching produces a simple rescaling of the lattice parameter, i.e., of the distance between carbons atoms. As a result, the new carbon–carbon distance under isotropic strain is $\mathbf{a}' = (\mathbf{I} + \boldsymbol{\epsilon}) \cdot \mathbf{a}$ and the new hopping parameter up to first-order in strain is $t' = t(1 - \beta\epsilon)$. Therefore, the new Fermi velocity obtained from the nearest-neighbor TB Hamiltonian is $v'_F = 3t'a'/2\hbar \simeq v_F(1 - \beta\epsilon + \epsilon)$. This result is not reproduced by the usual expansion around the old Dirac points as used in the pseudomagnetic field approach.[28]

Due to the utility of the uniform strain as a benchmark tool to test theories of strained graphene, here we calculate analytically the group velocity surfaces for such important case. Furthermore, this case can be solved without the usual perturbative analysis of the Dirac equation. For this goal, the TB approximation has been used. The Fermi velocities are obtained by looking at the appropriate points in the reciprocal space. Thus, our results are more general and include the Dirac theory of strain as a limiting case. Additionally, we found that even for a realistic value of pure shear strain, a mixed Dirac–Schrödinger behavior can arise, suggesting that the Dirac theory has to be modified. In fact, this behavior has been obtained in other cases.[7,29]

The layout of this paper is the following. In Sec. 2, we describe electron behavior in graphene under uniform strain. Then, a dispersion relation is obtained using the

TB approximation. For this relation, we display the surfaces and contour plots for the particular case of pure shear strain. In Sec. 3, we derive the group velocity for electrons and analyze the pure uniaxial and pure shear strain cases. Finally, in Sec. 4, we give our conclusions.

2. Electrons in Strained Graphene

Graphene is formed by a single atomic layer of carbon atoms arranged in a hexagonal structure. The structure can be described in terms of two triangular sub-lattices, A and B, with a basis of two atoms per unit cell. The lattice unit vectors are given by $\mathbf{a}_1$ and $\mathbf{a}_2$ and the three nearest-neighbor vectors can be written as $\boldsymbol{\delta}_1$, $\boldsymbol{\delta}_2$ and $\boldsymbol{\delta}_3$, as shown in Fig. 1(a). Likewise, there are two reciprocal-lattice vectors given by $\mathbf{b}_1$ and $\mathbf{b}_2$ and two inequivalent special points at the corners of the graphene BZ, called high symmetry points $\mathbf{K}_0$ and $\mathbf{K}'_0$. All these important points and a scheme of the unstrained graphene BZ are presented in Fig. 1(b) as an aid to the reader. For unstrained graphene, the tips of the Dirac cones (or the Dirac points $\mathbf{K}_D$) are located at the $\mathbf{K}_0$ and $\mathbf{K}'_0$ points.

In the case of a uniform strain, if the vector $\mathbf{r}$ represents the positions of the carbon atoms in the undeformed graphene, its deformed counterpart is given by $\mathbf{r}' = (\mathbf{I} + \boldsymbol{\epsilon}) \cdot \mathbf{r}$, where $\mathbf{I}$ is the 2×2 identity matrix and $\boldsymbol{\epsilon}$ is the uniform strain tensor. The lattice unit and nearest-neighbor vectors thus are $\mathbf{a}'_i = (\mathbf{I} + \boldsymbol{\epsilon}) \cdot \mathbf{a}_i$ $(i = 1, 2)$ and $\boldsymbol{\delta}'_n = (\mathbf{I} + \boldsymbol{\epsilon}) \cdot \boldsymbol{\delta}_n$ $(n = 1, 2, 3)$, while the reciprocal-lattice vectors are deformed as $\mathbf{b}'_i = (\mathbf{I} + \boldsymbol{\epsilon})^{-1} \cdot \mathbf{b}_i$ $(i = 1, 2)$. The new high symmetry points in the corners of the first BZ of the strained reciprocal lattice are obtained by construction of the Wigner–Seitz primitive cell. From geometrical arguments, it is easy to prove

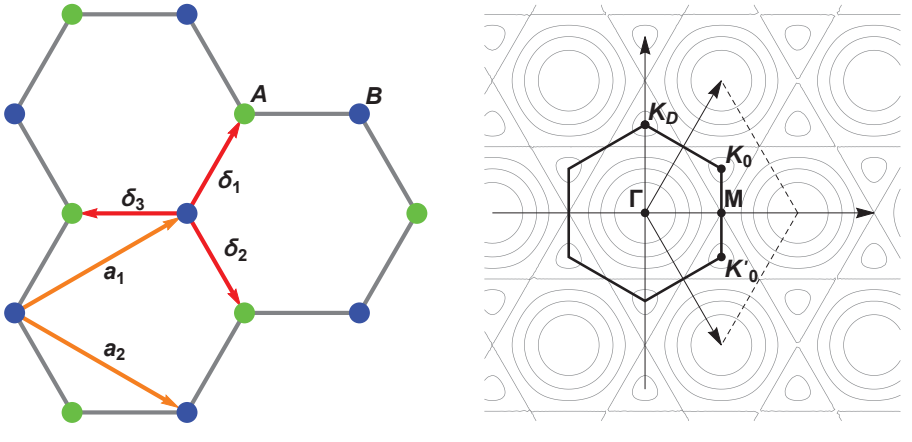

(a) (b)

Fig. 1. (Color online) (a) The unstrained graphene lattice and the sublattices A and B. The associated unitary and first neighbor vectors are also shown. (b) The scheme of the corresponding first BZ in reciprocal space showing the high symmetry points. The contours correspond to the energy surface.

that the new high symmetry points are given by

$$\mathbf{K} = \mathbf{M}_1^{-1}\mathbf{C}_1 \quad \text{and} \quad \mathbf{K}' = \mathbf{M}_2^{-1}\mathbf{C}_2\,, \tag{1}$$

with

$$\mathbf{M}_i = \begin{pmatrix} (b_i')_x & (b_i')_y \\ (b_1')_x + (b_2')_x & (b_1')_y + (b_2')_y \end{pmatrix}$$

and

$$\mathbf{C}_i = \frac{1}{2}\begin{pmatrix} \|\mathbf{b}_i'\| \\ \|\mathbf{b}_1' + \mathbf{b}_2'\| \end{pmatrix},$$

where $(b_i')_x$ and $(b_i')_y$ are the x- and y-components of the deformed reciprocal vectors $\mathbf{b}_i'$ $(i = 1, 2)$.

To obtain the electronic properties of graphene under uniform strain, we use the nearest-neighbor TB Hamiltonian[27]

$$\mathbf{H} = -\sum_{\mathbf{r}',n} t_n' \mathbf{a}_{\mathbf{r}'}^{\dagger} \mathbf{b}_{\mathbf{r}'+\boldsymbol{\delta}_n'} + \text{H.c.}\,, \tag{2}$$

where $\mathbf{r}'$ runs over all sites of the deformed honeycomb lattice and the hopping integral t_n' varies due to the modification in the carbon–carbon distances as $t_n' = t\exp[-\beta(|\boldsymbol{\delta}_n'|/a - 1)]$,[30] with $\beta \approx 3$ and $t \approx 2.7$ eV is the hopping energy for unstrained graphene.[6] The operators $\mathbf{a}_{\mathbf{r}'}^{\dagger}$ and $\mathbf{b}_{\mathbf{r}'+\boldsymbol{\delta}_n'}$ correspond to creating and annihilating electrons on the A sublattice position $\mathbf{r}'$ and B sublattice position $\mathbf{r}' + \boldsymbol{\delta}_n'$, respectively. Now, using the Fourier representation for these operators, the previous Hamiltonian can be written as[27]

$$\mathbf{H} = -\sum_{\mathbf{k},n} t_n' e^{-i\mathbf{k}\cdot(\mathbf{I}+\boldsymbol{\epsilon})\cdot\boldsymbol{\delta}_n} \mathbf{a}_{\mathbf{k}}^{\dagger}\mathbf{b}_{\mathbf{k}} + \text{H.c.}\,, \tag{3}$$

which finally leads to the closed dispersion relation for graphene under uniform strain[27]

$$E(\mathbf{k}) = \pm\left\|\sum_n t_n' e^{-i\mathbf{k}\cdot(\mathbf{I}+\boldsymbol{\epsilon})\cdot\boldsymbol{\delta}_n}\right\|. \tag{4}$$

For the purposes of this work, it is useful to rewrite Eq. (4) in a more explicit way. We start by writing the norm in Eq. (4) as

$$E(\mathbf{k}) = \pm\left(\sum_n t_n' e^{-i\mathbf{k}\cdot(\mathbf{I}+\boldsymbol{\epsilon})\cdot\boldsymbol{\delta}_n}\right)\left(\sum_s t_s' e^{i\mathbf{k}\cdot(\mathbf{I}+\boldsymbol{\epsilon})\cdot\boldsymbol{\delta}_s}\right). \tag{5}$$

By splitting the resulting sum into terms with $n = s$ and $n \neq s$, this leads to

$$E(\mathbf{k}) = \pm\sqrt{\gamma + g(\mathbf{k})}\,, \tag{6}$$

where

$$g(\mathbf{k}) = \sum_{n=1}^{3}\sum_{s>n}^{3} 2t_n' t_s' \cos[\mathbf{k}\cdot(\mathbf{I}+\boldsymbol{\epsilon})\cdot(\boldsymbol{\delta}_n - \boldsymbol{\delta}_s)]$$

and

$$\gamma = \sum_{n=1}^{3} t_n'^2 \,.$$

The obtained expression Eq. (6) turns out to be very useful because it allows a straightforward analytical evaluation of the energy and velocity surfaces, as we will show in the rest of the paper. Let us start by exploring the strain effects on the energy dispersion relation. As explained previously, when a uniform strain is applied the reciprocal lattice is also strained. Thus, the first BZ is modified, i.e., its original hexagonal form is varied to a polygonal form, as shown for the particular cases of pure shear strain along the armchair direction: $\epsilon_{xx} = \epsilon_{yy} = 0$, $\epsilon_{xy} = \epsilon_{yx} = 0.1$ [see red lines Fig. 2(a)] and $\epsilon_{xy} = \epsilon_{yx} = 0.2$ [see red lines Fig. 2(b)]. In the same Fig. 2, along with the first BZ, we present the contour plot of the energy obtained from Eq. (6).

Once the first BZ and the energy surfaces are obtained, we need to locate the Dirac points $\mathbf{K}_D$ using the condition $E(\mathbf{K}_D) = E_F$, which corresponds to electrons at the Fermi level. By applying this condition, the Dirac points are indicated as pink circles in Fig. 2. The most important conclusion from the figure is that such points are no longer located at the high symmetry points $\mathbf{K}$ and $\mathbf{K}'$ (red circles) of the corners of the first BZ [Eq. (1)], since they are shifted to the saddle point. In fact, the separation of the Dirac points from the high symmetry points revealed

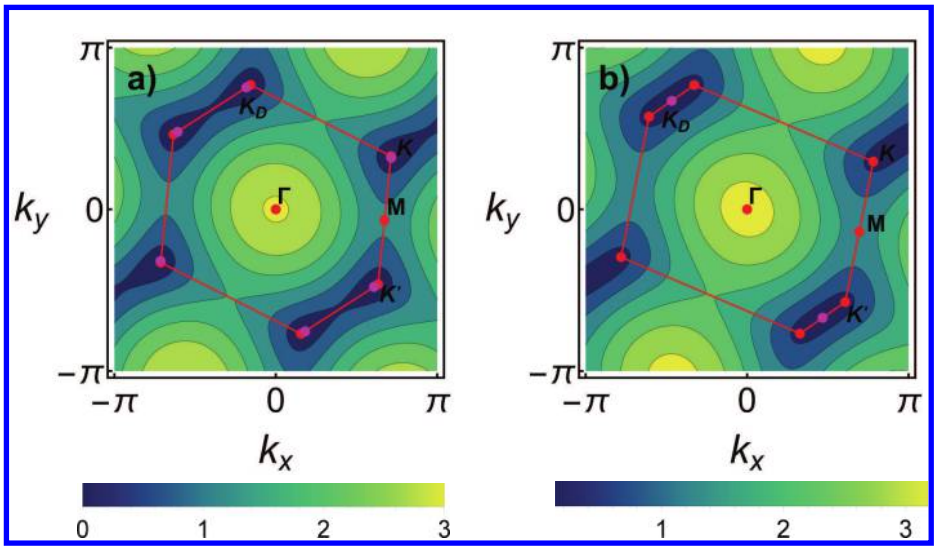

Fig. 2. (Color online) Contour plots of the energy for a shear strain given by $\epsilon_{xx} = \epsilon_{yy} = 0$ and with (a) $\epsilon_{xy} = 0.1$ and (b) $\epsilon_{xy} = 0.2$. The first BZ of the strained reciprocal lattice is presented with red lines. The high symmetry points $\mathbf{K}$ and $\mathbf{K}'$ [Eq. (1)] are indicated with red circles. The pink circles correspond to the position of the Dirac cones $\mathbf{K}_D$, where the Fermi energy is located. Notice how two Dirac cones merges into one in case (b) and do not have the same position as $\mathbf{K}$ and $\mathbf{K}'$.

by Fig. 2 has been mostly disregarded in several papers available in the literature, although it has been reported in some carefully made works.[10,12]

As deformation increases (up to 20%), the Dirac points merge into the saddle point and a gap opens, which is consistent with the results in references.[7,32] Furthermore, in this critical point, the dispersion relation is linear along one direction ((relativistic Dirac behavior) and quadratic along the other one (nonrelativistic Schrödinger behavior). Therefore, the Dirac theory needs to be modified.

Summarizing the above, the effects caused in graphene under uniform strain are the following:

- The Dirac points are shifted from the corners of the strained BZ.
- The Dirac equation is no longer suitable for long strain ($\geq 20\%$), since for particular cases a Dirac–Schrödinger behavior is observed and furthermore one might expect significant nonlinear corrections. It follows that the anisotropic Fermi velocity is no longer valid in these regimens. Therefore, we must consider a more general velocity to understand the electron behavior. This is done through the calculation of the group velocity, as we will discuss in the following section.

3. Group Velocity

In the literature, the basic properties of electron transport phenomena in a crystal are described in terms of Bloch waves with wave vectors $\mathbf{k}$.[31] Using these waves, we can build a dispersive wave packet with a certain group velocity. It can be shown quite generally that the mean electron velocity is given by the group velocity of the wave packet[31]

$$\mathbf{v}(\mathbf{k}) = \nabla_{\mathbf{k}} E(\mathbf{k})\,, \tag{7}$$

where $\nabla_{\mathbf{k}}$ is the gradient operator in $\mathbf{k}$-space.

From this equation, the real-space motion of the electron can be described. Here we are interested in the behavior of electrons in graphene under uniform strain. Thus, by substituting Eq. (6) into Eq. (7) we obtain

$$\mathbf{v}(\mathbf{k}) = \pm\frac{1}{2E(\mathbf{k})}\nabla_{\mathbf{k}} g(\mathbf{k})\,. \tag{8}$$

The components x and y of $\mathbf{v}(\mathbf{k})$ are given by

$$v_l(\mathbf{k}) = \pm\sum_{n=1}^{3}\sum_{s>n}^{3}[(1+\epsilon_{ll})(\delta_n^l - \delta_s^l) + \epsilon_{lm}(\delta_n^m - \delta_s^m)] \times t'_n t'_s \frac{\sin[\mathbf{k}\cdot(\mathbf{I}+\boldsymbol{\epsilon})\cdot(\boldsymbol{\delta}_n - \boldsymbol{\delta}_s)]}{\sqrt{\gamma + g(\mathbf{k})}}\,, \tag{9}$$

where l, $m = \{x, y\}$ and $l \neq m$. The group velocity norm is given by $v(\mathbf{k}) = |\mathbf{v}(\mathbf{k})|$. In Fig. 3, we plot the surfaces and contour of the group velocity norm $v(\mathbf{k})$ for pure graphene. It is important to note that at low energies and in the vicinity of

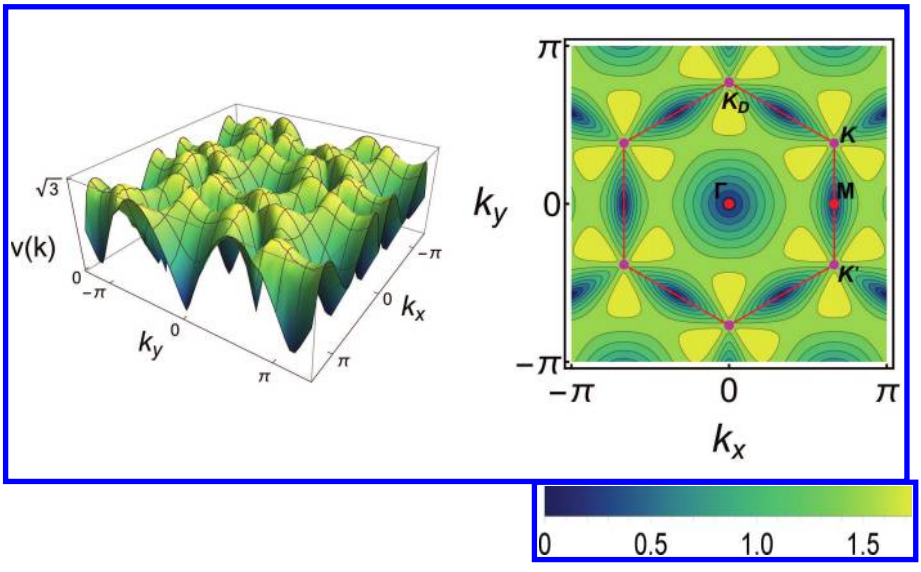

Fig. 3. (Color online) (a) Surface and (b) contour plots of the group velocity norm for pure graphene. Notice the three lobules centered at the high symmetry points, which arise when nonlinear terms are included in the expansion of the energy around these points.

the Dirac points, $v(\mathbf{k})$ is isotropic, coinciding with the Fermi velocity. However, as we move away from the Dirac point (corresponding to nonlinear corrections to the Dirac cone) a trigonal warping appears, giving rise to an anisotropic behavior, corresponding to the lobes seen in Fig. 3. Furthermore, it can be observed that in the directions where the trigonal warping appear, $v(\mathbf{k})$ increases, while in other directions it decreases drastically. These results do not appear when the Dirac theory is used. Therefore, if we want a complete understanding of the behavior of electrons in the energy bands, nonlinear corrections and directions should be considered, since strain effects enhance these features, as we discuss below.

We analyze the particular cases of pure uniaxial and pure shear strain along the armchair direction: $\epsilon_{xy} = \epsilon_{yy} = 0$, $\epsilon_{xx} = 0.1, 0.2$ and $\epsilon_{xx} = \epsilon_{yy} = 0$, $\epsilon_{xy} = 0.1, 0.2$, as shown in Figs. 4 and 5, respectively. In Figs. 4 and 5, the contour plots of the velocity norm $v(\mathbf{k})$ are presented. Over imposed to these contours, we present the first BZ of the strained reciprocal lattice with red lines. Likewise, the high symmetry points [Eq. (1)] are indicated with red circles. The pink circles correspond to the position of the Dirac points $\mathbf{K}_D$ where the Fermi energy is located. Notice again how the $\mathbf{K}_D$ points do not have the same position as the high symmetry points $\mathbf{K}$ and $\mathbf{K}'$. This effect is much more pronounced for shear strain.

On the other hand, the effects caused by the deformation in the velocity surfaces are the following:

- As seen in Figs. 4 and 5, the Fermi velocity is no longer isotropic. Instead, it becomes strongly anisotropical. This is seen by inspecting the neighborhoods of the Dirac points, i.e., the pink dots in Figs. 4 and 5.

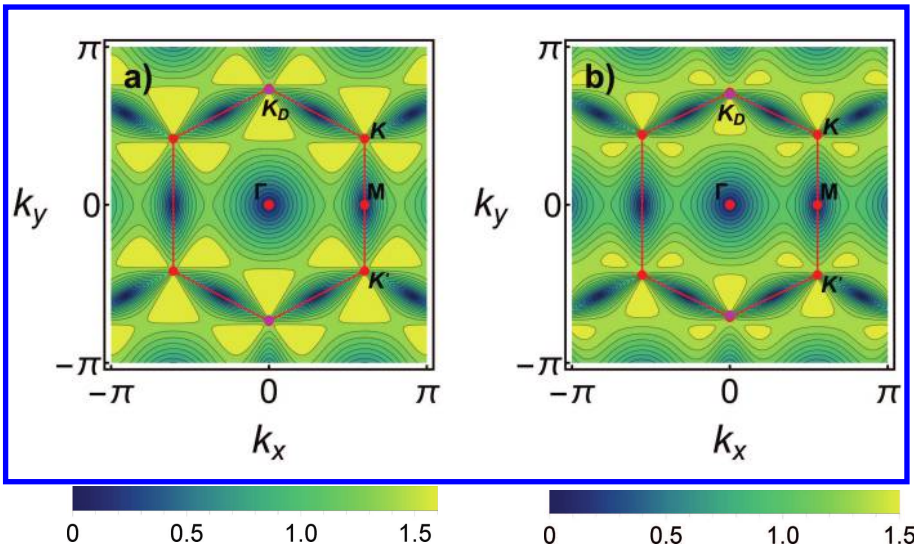

Fig. 4. (Color online) Contour plots of the group velocity for a uniaxial uniform strain given by $\epsilon_{xy} = \epsilon_{yy} = 0$ and with (a) $\epsilon_{xx} = 0.1$ and (b) $\epsilon_{xx} = 0.2$. The first BZ of the strained reciprocal lattice is presented with red lines. The high symmetry points $\mathbf{K}$ and $\mathbf{K}'$ [Eq. (1)] are indicated with red circles. The pink circles correspond to the position of the Dirac cones $\mathbf{K}_D$, where the Fermi energy is located. Notice how $\mathbf{K}_D$ do not have the same position as $\mathbf{K}$ and $\mathbf{K}'$.

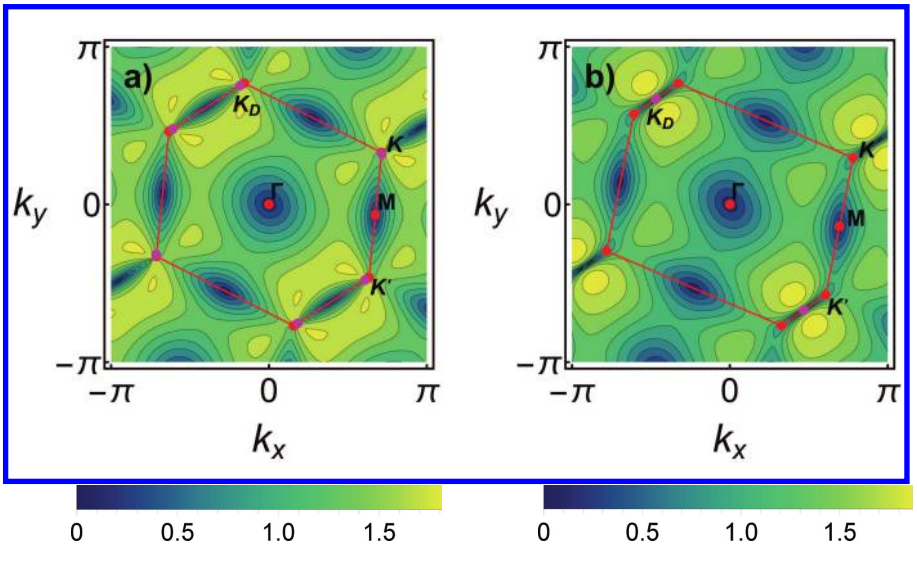

Fig. 5. (Color online) Contour plots of the group velocity for a shear strain given by $\epsilon_{xx} = 0$, $\epsilon_{yy} = 0$ and with (a) $\epsilon_{xy} = 0.1$ and (b) $\epsilon_{xy} = 0.2$. The first BZ of the strained reciprocal lattice is presented with red lines. The high symmetry points $\mathbf{K}$ and $\mathbf{K}'$ [Eq. (1)] are indicated with red circles. The pink circles correspond to the position of the Dirac cones $\mathbf{K}_D$, where the Fermi energy is located. Notice how two Dirac cones merge in case (b) and do not have the same position as $\mathbf{K}$ and $\mathbf{K}'$. From the contour plot, it is clear that the Fermi velocity is constant (Dirac behavior) in the principal axis of the shear, while it follows a parabolic (Schrödinger) behavior in the perpendicular direction.

- The surfaces do not display the trigonal symmetry anymore, instead they present the symmetry of the corresponding strained reciprocal lattice.
- For uniaxial strain, the non-linear trigonal warping lobes observed around the Dirac cones in pure graphene are strongly modified as seen in Fig. 4. The new lobes follow the symmetry of the strained reciprocal lattice, i.e., the angles between them are no longer 120°. This new warping is strongly spatially modulated. Furthermore, some lobes can even touch the Dirac points as occuring in Fig. 4(b). Since the warping is associated with nonlinear terms, this shows that nonlinearity is important in order to describe such cases. As a result, a pure Dirac equation is no longer valid.
- For shear strain, the results are similar. As seen in Fig. 5(a), the nonlinear trigonal warping lobes are deformed. In Fig. 5(b), the three lobes merge into two lobules reflecting the symmetry of the strained reciprocal space.
- When the Dirac cones merge by shear strain as in Fig. 5(b), the group velocity is zero along one of the principal axis of the deformation. This is just the consequence of the energy having a parabolic (Schrödinger) behavior with a gap opening.[7] This effect has also been documented when periodic uniaxial strain is applied,[29] as found by using a nonperturbative approach that maps the problem to a one-dimensional effective chain.[29,33] This effective chain has a complex spectrum due to its similarity with other quasiperiodic or modulated systems.[34–37]

4. Conclusions

By deriving a simplified expression for the energy dispersion surface, we obtained the electron group velocity for graphene under uniform strain using the TB approximation. Our results indicate that the velocity is strongly anisotropic and that the trigonal warping is deformed to follow the symmetry of the strained reciprocal lattice. As strain increases, this warping touches the Dirac points. Thus, we found that nonlinearity is very important in order to describe electrons in a proper way near the Fermi energy, since the trigonal warping observed in graphene touches the Dirac point and gets modulated by the symmetry of the strained reciprocal lattice. As a result, a Dirac equation kind of approximation is no longer valid for such cases. In fact, our results suggest the need for a dual Schrödinger–Dirac equation, in the sense that its character must depend on the direction, as a starting point for effective equations in shear strain.

Finally, our closed analytical expressions for the electron velocities are useful in order to calculate the electronic, thermal and optical properties of strained graphene. For example, the electronic conductivity will be modified, leading to a modulated optical reflectivity, transmittance and a modified Raman response, as has been documented recently.[38] Another interesting question is how the underlying wavefunction frustration present in graphene is modified by strain,[39,40] as well as the multifractal properties of the wavefunctions for doped graphene.[41]

Acknowledgments

G. Naumis thanks the program DGAPA-PASPA for the sabbatical scholarship. W. Gómez-Arias thanks CONACyT for the master scholarship. This work was funded by DGAPA-PAPIIT project IN-102513. Calculations were performed at DGTIC-UNAM Center.

References

1. K. S. Novoselov *et al.*, *Science* **306**, 5696 (2004).
2. A. K. Geim, *Nature Mater.* **6**, 3 (2007).
3. S. Das Sarma *et al.*, *Solid State Commun.* **143**, 12 (2007).
4. A. K. Geim, *Science* **324**, 5934 (2009).
5. K. S. Novoselov, *Rev. Mod. Phys.* **83**, 3 (2011).
6. A. H. C. Neto *et al.*, *Rev. Mod. Phys.* **81**, 1 (2009).
7. V. M. Pereira, A. H. C. Neto and N. M. R. Peres, *Phys. Rev. B* **80**, 4 (2009).
8. F. Guinea, *Solid State Commun.* **152**, 15 (2012).
9. G. Cocco, E. Cadelano and L. Colombo, *Phys. Rev. B* **81**, 24 (2010).
10. I. I. Naumov and A. M. Bratkovsky, *Phys. Rev. B*, **84**, 2424544 (2011).
11. S. H. R. Sena *et al.*, *J. Phys.: Condens. Matter* **306**, 5696 (2004).
12. N. Kerszberg and P. Suryanarayana, *RSC Adv.* **5**, 43810 (2015).
13. V. M. Pereira and A. H. C. Neto, *Phys. Rev. Lett.* **103**, 4 (2009).
14. Y. Jiang *et al.*, *Phys. Rev. Lett.* **110**, 4 (2013).
15. D. A. Gradinar *et al.*, *Phys. Rev. Lett.* **110**, 26 (2013).
16. S. Barraza-Lopez *et al.*, *Solid State Commun.* **166**, 70 (2013).
17. H. H. Nguyen, V. V. Nguyen and P. P. Dollfus, *Nanotechnology* **25**, 16 (2014).
18. R. Winkler and U. Zülicke, *Phys. Rev. B* **82**, 24 (2010).
19. T. L. Linnik, *J. Phys.: Condens. Matter* **24**, 205302 (2012).
20. J. V. Sloan *et al.*, *Phys. Rev. B* **87**, 15 (2013).
21. F. Guinea, *Physica B* **407**, 15 (2012).
22. R. Kerner, G. G. Naumis and W. A. Gomez-Arias, *Solid State Commun.* **152**, 12 (2012).
23. A. A. P. Sanjuan *et al.*, *ACS Nano* **8**, 2 (2014).
24. A. A. P. Sanjuan *et al.*, *Phys. Rev. B* **89**, 12 (2014).
25. A. L. Kitt *et al.*, *Phys. Rev. B* **85**, 11 (2012).
26. A. L. Kitt *et al.*, *Phys. Rev. B* **87**, 159909 (2013).
27. M. Oliva-Leyva and G. G. Naumis, *Phys. Rev. B* **88**, 8 (2013).
28. F. de Juan, M. Sturla and M. A. H. Vozmediano, *Phys. Rev. Lett.* **108**, 227205 (2012).
29. P. Roman-Taboada and G. G. Naumis, *Phys. Rev. B* **90**, 195435 (2014).
30. R. M. Ribeiro *et al.*, *New J. Phys.* **11**, 115002 (2009).
31. U. Mizutani, *Introduction ot the Electron Theory of Metals* (Cambridge University Press, 2001).
32. G. Montambaux *et al.*, *Phys. Rev. B* **80**, 153412 (2009).
33. G. G. Naumis and P. Roman-Taboada, *Phys. Rev. B* **89**, 241404(R) (2014).
34. J. C. Lopez, G. G. Naumis and J. L. Aragon, *Phys. Rev. B*, **48**, 12459 (1993).
35. G. G. Naumis, *Phys. Rev. B* **59**, 11315 (1999).
36. G. G. Naumis and J. L. Aragón, *Phys. Rev. B* **54**, 15079 (1996).
37. I. Satija and G. G. Naumis, *Phys. Rev. B* **88**, 054204 (2013).
38. C. Neumann *et al.*, *Nature Commun.* **6**, 8429 (2015).

39. G. G. Naumis, *Phys. Rev. B* **76**, 153403 (2007).
40. J. E. Barrios-Vargas and G. G. Naumis, *J. Phys.: Condens. Matter* **23**, 375501 (2011).
41. J. E. Barrios-Vargas and G. G. Naumis, *2D Mater.* **1**, 011009 (2014).